Flattening-filter-based empirical methods to parametrize the head scatter factor

Kwok L. Lam, Moorthy S. Muthuswamy, and Randall K. Ten Haken
Department of Radiation Oncology, University of Michigan, Ann Arbor, Michigan 48109-0010

(Received 28 September 1994; resubmitted 7 August 1995; accepted for publication 25 October 1995)

87.53.10.h
87.54.01

Parametrizing the collimator scatter factor, S_c (or head scatter factor), of a linear accelerator by the side of the equivalent square of the collimator setting at the isocenter does not accurately predict the change in S_c when the width and length of a rectangular field are exchanged. We have studied two methods based on measurements of square fields to predict S_c's of rectangular fields more accurately. The first method parametrizes S_c by the side of the equivalent square of the flattening filter region visible from the point of calculation. The S_c's of rectangular fields were predicted to an accuracy of 1% from measurements with square fields. The second method computes S_c of rectangular configurations by integrating radiation that can reach the point of calculation from a point source at the target and a second extended source at the flattening filter. The radial distribution of the extended source at the level of the flattening filter is computed from S_c of square fields measured at the isocenter. Effects of extended distance are modeled by separately performing inverse square law corrections for the two sources. This method also predicted the measured values to within 1% accuracy. © *1996 American Association of Physicists in Medicine.*

Key words: head scatter, output factor, collimator scatter factor, equivalent square, radial distribution

I. INTRODUCTION

The collimator scatter factor, S_c,[1-2] is conventionally parametrized with the adjustable collimator settings at a fixed reference distance, i.e., at the isocenter. It is approximately independent of the distance between the source and the calculation point (source-to-point distance, SPD).[2-4] It is usually experimentally determined as a function of the square field sizes at the isocenter. The S_c values for rectangular fields are then estimated by computing the equivalent square of the same area to perimeter ratio and the S_c corresponding to the equivalent square is taken to be the S_c of the rectangular field. It is well known that S_c of two rectangular fields with width and length exchanged are different.[5-10] If accurate S_c are desired, they must be measured for different combinations of width and length of the radiation field.

The physical origin of S_c has been studied extensively.[6,7,11-14] It is mainly due to the change in scattered radiation that can reach the point of measurement as the position of the collimators is varied (Fig. 1). The sources of scattered radiation are structures inside the head of the linear accelerator. Although S_c has been designated as the collimator scatter factor, the collimator is not the main source of the scattered radiation. Major sources are structures close to the target. The flattening filter has been suggested as one of the major sources of scattered radiation.[7,11,13,14] Recently, the photon energy fluence reaching the point of calculation has been modeled as the sum of energy fluences from two sources: a point source at the target and an extended source at the flattening filter.[15-18] The photon energy fluence at the point of measurement from each unit area on the filter has been modeled as uniform,[15] triangular,[19] and Gaussian,[16] as well as determined experimentally with special collimation.[17,18]

In this study, two methods to parametrize S_c were compared with the method using the equivalent square at the isocenter. In the first method, the equivalent square of the flattening filter region visible from the point of measurement was used to parametrize the amount of scattered radiation detected under various field shapes and distances. In the second method, the radial distribution of scattered radiation at the flattening filter was determined from square field measurements without any special equipment. Then S_c was computed by numerical integration.

II. MATERIALS AND METHODS

A. Experimental methods

1. Dependence of scatter on collimator setting

Dependence of scatter on collimator settings was measured with a cylindrical solid water mini-phantom as described by van Gasteren *et al.*[3] The measurements were taken on a Varian 2100C with 6- and 15-MV photons. The mini-phantom was 4 cm in diameter and 13.2 cm long. A 0.14-cm^3 air ionization chamber was mounted axially inside the mini-phantom with the center of the sensitive volume, taken to be the location of the measurement point, at 10 cm from the front surface. The chamber was chosen because of its small volume. The effect of electron contamination was minimal at 10-cm depth for the x-ray beams investigated in this study. Thus, the results reflect the effect of collimator opening on dose due to x rays. All measurements were performed with the ionization chamber in a mini-phantom (supported by a low density polystyrene-foam holder) oriented along the rotation axis of the collimator.

 0094-2405/96/23(3)/343/10/$6.00

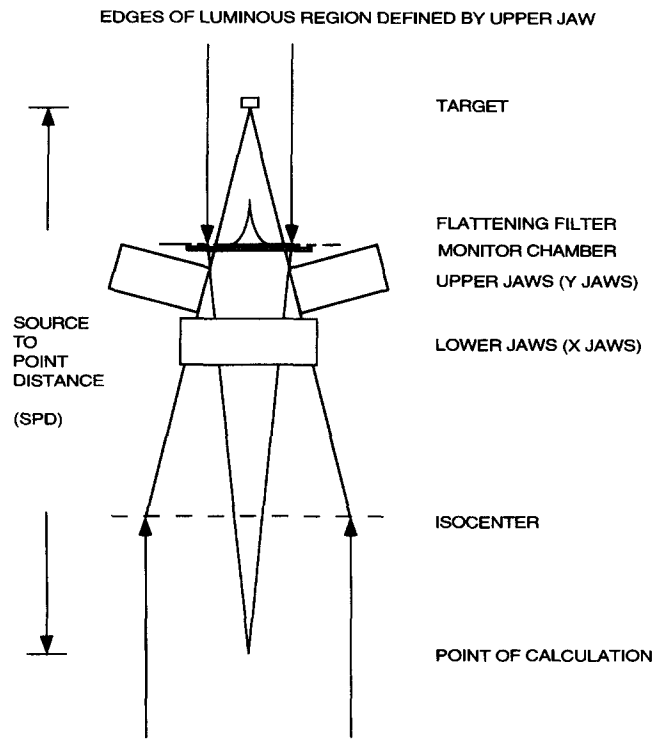

FIG. 1. Schematic diagram showing the geometrical relationship among the point of calculation, the jaw settings, field size at isocenter, and the luminous region at the bottom of the flattening filter.

In the experiment, two sets of data were taken. The first-dataset consisted of charge measurements $Q_c(r_x,r_y,SPD)$ for lower jaw setting r_x and upper jaw setting r_y of square field sizes from 5–40 cm with source-to-measurement-point distance (abbreviated as source-to-point distance, SPD) of 100 cm to estimate the parameters required in the methods. The second dataset was used to test the accuracy of the methods in predicting the measurements of different field configurations. The test field configurations chosen were (i) SPD at 100 cm, (a) rectangular fields with r_x at 40 cm and r_y varied between 5–40 cm and (b) rectangular fields with r_y at 40 cm and r_x varied between 5–40 cm; (ii) SPD at 160 cm, (a) square fields from 3–29 cm (b) rectangular fields with r_x at 40 cm and r_y varied between 3–20 cm, and (c) rectangular fields with r_y at 40 cm and r_x varied between 3–20 cm.

2. Backscatter into monitor chamber

Backscatter into monitor chamber[5,6,8,13,15,20,21] was measured with the telescopic method of Kubo.[20] The telescope was formed by the multileaf collimator (MLC), a low-melting-point-metal alloy (cerrobend) block mounted below a tray on the accessory mount, a cerrobend block hand placed above the same tray, and a cerrobend housing around the ionization chamber on the floor. The cerrobend blocks mounted above and below an accessory mount tray were both 7.5-cm thick. The larger cerrobend block mounted below the tray did not block the area already shielded by the MLC, so that its weight was significantly reduced. A 0.95-cm hole was drilled at the center of this block. The smaller block with a 0.52-cm hole at the center was hand placed on top of the tray to align the hole with the central axis. The solid cerrobend ionization chamber housing was also made of a stack of two 7.5-cm-thick cerrobend blocks. The ionization chamber was the same chamber used above. The chamber was placed inside a 1-mm-thick plastic cap mainly for physical protection. The upper block of the housing had a 0.52-cm hole at the center forming part of the telescope. The lower block had a channel on its surface for the ionization chamber and its cap. Charges $Q_b(r_x,r_y)$ collected by the chamber were measured with r_x at 38 cm and r_y varied between 3 and 38 cm as well as r_y at 38 cm and r_x varied between 3 and 38 cm. The holes in the blocks mounted on the accessory mount were then plugged (filled back in with cerrobend) and the measurements repeated to estimate the background scatter $Q_s(r_x,r_y)$ into the ionization chamber.

B. Methods of data reduction

1. Traditional parametrization with the equivalent square at isocenter

From the measured $Q_c(r_x,r_y,SPD)$, we define the relative fluence factor, RFF, as

$$RFF(r_x,r_y,SPD)=\frac{Q_c(r_x,r_y,SPD)}{Q_c(r_0,r_0,SPD_0)}, \tag{1}$$

where SPD_0 is the SPD of the reference configuration. In this study, r_0 and SPD_0 were taken to be 40 and 100 cm, respectively. Here r_0 was chosen to be 40 cm because the dependence of the data on the field size was minimum at this field size so that small error in field size would not translate as much into measurement error. This factor includes both the distance dependence and collimator setting dependence of the measured charge.

According to Tatcher and Bjarngard[4] and McKenzie and Stevens,[22] the distance dependence can be closely approximated by the inverse-square law for a single effective source at a short distance t_e downstream of the target. For parametrization versus the side of equivalent square at isocenter r_c, S_c can be written as

$$S_c(r_c)=\frac{RFF(r_x,r_y,SPD)}{\left(\frac{SPD_0-t_e}{SPD-t_e}\right)^2}. \tag{2}$$

When SPD is equal to SPD_0, S_c is reduced to RFF, which is then reduced to $Q(r_x,r_y,SPD_0)/Q(r_0,r_0,SPD_0)$, identical to the conventional definition of S_c. Thus, we can determine the dependence of S_c on r_c from RFF for square fields at 100-cm SPD. Linear interpolation was used to obtain S_c for r_c between measured values. We identified this $S_c(r_c)$ as the parametrized S_c. To determine t_e, we adjusted t_e in Eq. (2) until the root-mean-square deviation between S_c at 160 cm and the parametrized S_c was minimized. For other field configurations, deviations of measured S_cs from parametrized S_c were then computed.

2. Backscatter into monitor chamber

Part of the collimator dependence of S_c is due to radiation backscattered into the monitor chamber. Since backscatter does not depend on SPD and its dependence on collimator settings is different from that of scattered radiation from the head to the calculation point, we have decomposed S_c into a product of two factors:[6,8,13] one for the backscatter into the monitor chamber S_b (monitor backscatter factor) and one for the head scatter to the calculation point S_h (head scatter factor). That is,

$$S_c = S_b S_h . \tag{3}$$

Hereafter we will reserve the term head scatter factor for this more restricted sense.

The background scatter in the S_b measurement with the telescopic method was assumed to be a linear function of the area of the field size at isocenter. Thus, the charge measured with the holes at the accessory mount plugged were fitted by linear least squares fit to

$$Q_s(r_x, r_y) = e_0 + e_1 r_x r_y , \tag{4}$$

where e_0 and e_1 were fitting constants. The charge measured with the telescopic setup was then corrected for background scatter by subtracting $Q_s(r_x, r_y)$ from the measurements $Q_b(r_x, r_y)$.

We define the monitor backscatter factor $S_b(r_x, r_y)$ as the ratio of the amount of x-ray photon energy generated at the target for a field size of (r_x, r_y) to that generated for the reference field size (r_0, r_0). Therefore,

$$S_b = \frac{1}{[Q_b(r_0, r_0) - Q_s(r_0, r_0)]} [Q_b(r_x, r_y) - Q_s(r_x, r_y)]. \tag{5}$$

We have taken r_0 to be 40 cm in this study. The data can easily be renormalized to a different r_0, such as 10 cm, if necessary.

From Appendix A, it is shown that $S_b(r_x, r_y)$ can be modeled as

$$S_b(r_x, r_y) = c_0 + c_1 r_y + c_2 r_x r_y . \tag{6}$$

Since $[Q_b(r_x, r_y) - Q_s(r_x, r_y)]$ is proportional to S_b, we have fitted $[Q_b(r_x, r_y) - Q_s(r_x, r_y)]$ to the bilinear equation above by linear least squares fit. It was then normalized to unity for a 40-cm square collimator setting to obtain S_b.

3. Parametrization with the equivalent square at flattening filter

The head scatter factor (S_h) depends on the scattered radiation from components of the treatment head to the point of calculation. Therefore, head scatter factors depend on the visible region of the scattering components from the point of view of the calculation point.[5,7,15,16,18] Since the flattening filter is the major source of scattered radiation, we project all sources of scattered radiation to the level of the flattening filter from the point of calculation. We will denote the visible region projected to the flattening filter as the luminous region. The geometrical relationship of the point of calculation to the different structures in the head defining the luminous region is illustrated schematically in Fig. 1. As can be seen from Fig. 1, for a given collimator setting, the size of the luminous region depends also on SPD. We have neglected the scattered radiations from the collimator jaws when we define the luminous region.

For parametrization versus the side of equivalent square of the luminous region r_l, S_h can be written as

$$S_h(r_l) = \frac{RFF(r_x, r_y, SPD)}{\left(\frac{SPD_0 - t_e}{SPD - t_e}\right)^2 S_b(r_x, r_y)} . \tag{7}$$

Similar to the reduction for $S_c(r_c)$, the parametrized S_h was determined from square field data at 100-cm SPD and linear interpolation, and then t_e was obtained by minimizing the root-mean-square deviation between S_h of square fields at 160-cm SPD and parametrized S_h. Deviations of measured S_h for other field configurations from parametrized S_h were then obtained.

4. Parametrization with the integral of the radial distribution

Following the concept of the two-source model developed recently,[15–18] if we assume that the scattered radiation distribution is radially symmetric, we can write RFF

$$RFF(SPD, r_x, r_y, \sigma) = S_b(r_x, r_y)\left[\left(\frac{SPD_0}{SPD}\right)^2 \lambda_t + \left(\frac{SPD_0 - t_f}{SPD - t_f}\right)^2 \int\int_{\sigma} \lambda(R)\, dA\right], \tag{8}$$

where σ is the luminous region, t_f is the distance of the flattening filter from the target, λ_t represents the point source at the target, and $\lambda(R)$ represents the radial distribution of the scattered radiation at the luminous region. Here λ_t and $\lambda(R)$ are normalized so that the factor in square brackets is unity for σ_0, the luminous region of the reference field configuration. Physical interpretations of λ_t and $\lambda(R)$ are shown in Appendix B.

In this study, we have employed a method to determine the radially symmetric distribution $\lambda(R)$ and the point source λ_t from conventional mini-phantom in-air measurements for different square field sizes at isocenter. If we define q to be RFF/S_b, which can be measured experimentally, then from Eq. (8)

$$q(\sigma) = \left(\frac{SPD_0}{SPD}\right)^2 \lambda_t + \left(\frac{SPD_0 - t_f}{SPD - t_f}\right)^2 \int\int_{\sigma} \lambda(R)\, dA. \tag{9}$$

The problem is reduced to solving this integral equation for $\lambda(R)$ from measured $q(\sigma)$.

For a set of m different field shapes σ_i, $i = 1,2,\ldots,m$, there are m corresponding q_i from the in-air measurement at SPD_i. In the data reduction, only measurements q_i of square

collimator settings with SPD of 100 cm were used. The determination of $\lambda(R)$ from measurements q_i of its integral is sensitive to random error,[17] because some form of differentiation, either directly or indirectly, is needed to solve for the integrand from the integral. To reduce the effect of random error, q_i as a function of collimator settings were first smoothed by discrete-cubic-spline fitting. The amount of smoothing was controlled by adjusting the weights of the data points. The spline will meander through noisy data points if they are given strong weights. The weights of individual data points were adjusted until the root-mean-square deviation of a fitted curve with continuously decreasing positive slope from the data points was minimized. It is shown in Appendix C that λ_t and $\lambda(R)$ can be solved numerically from the fitted spline $q(\sigma)$ by transforming Eq. (9) to a system of linear equations.

The RFFs for different collimator configurations and/or SPD were then computed from Eq. (8) and deviations of computed RFFs from measured RFFs were obtained.

III. RESULTS

A. Traditional parametrization with the equivalent square at isocenter

In Fig. 2, measured S_c [Eq. (2)] for both square fields and rectangular fields are plotted against the side of equivalent square at isocenter. Standard deviation of measurements taken on different days and at different times for 10-cm by 10-cm field size of the 6-MV photon beam was 0.1%. It is shown in Fig. 2(a) as an error bar. This indicates the precision of the measurements since we have normalized S_c to unity for a 40-cm square field. In Fig. 2, the deviation of measured S_c from parametrized S_c was systematic. Thus, the maximum deviation was used as a measure of deviation. It was 1.7% for 6 MV and 1.9% for 15 MV. The effective source was 1.4 cm downstream of the target for 6 MV and 0.8 cm downstream for 15 MV.

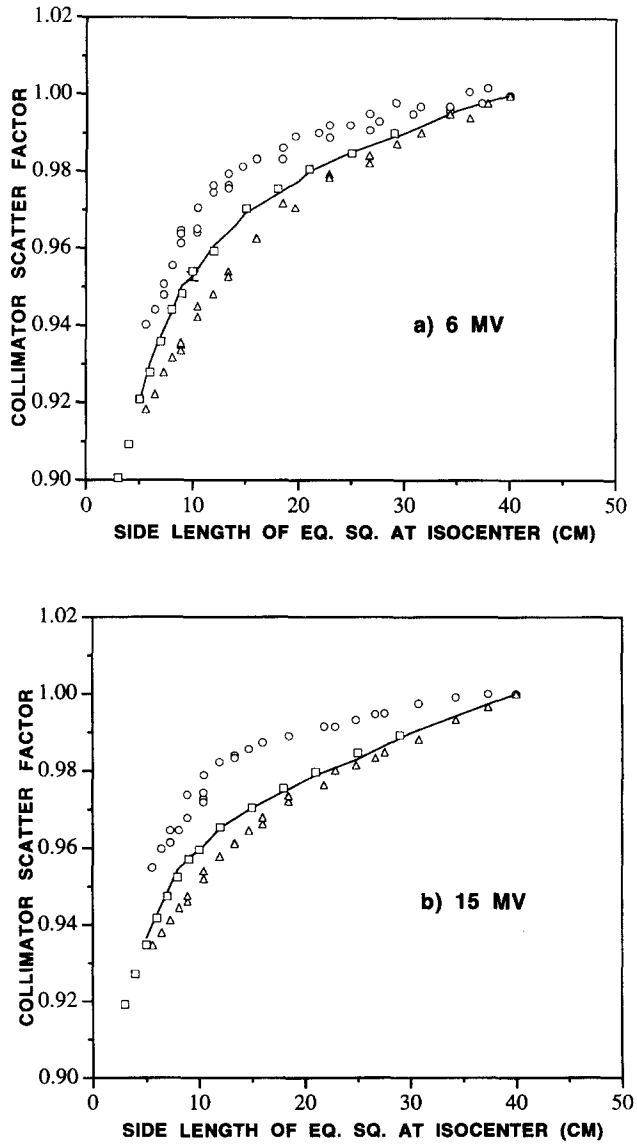

FIG. 2. Collimator scatter factor S_c using conventional method of data analysis. Solid line is the parametrized S_c. It is the linear interpolation of S_c of square fields at 100-cm target-to-measurement-point distance. Squares are data points of square fields at 160 cm. Triangles are data points of rectangular fields with different upper jaw settings and lower jaws at 40 cm. Circles are data points of rectangular fields with different lower jaw settings and upper jaws at 40 cm. Data at 100 and 160 cm were included in the data set of rectangular fields. The error bar at collimator setting of 10 cm for 6 MV indicates one standard deviation of the measurements.

B. Backscatter into monitor chamber

The monitor backscatter factor for lower jaws at 38 cm and upper jaws varied as well as upper jaws at 38 cm and lower jaws varied are shown in Fig. 3. The backscatter measurements yielded parameters c_0, c_1, and c_2 in Eq. (6) of $(0.9783\pm0.5\times10^{-3})$, $(0.36\times10^{-3}\pm0.2\times10^{-4})$ cm^{-1}, and $(0.45\times10^{-5}\pm0.5\times10^{-6})$ cm^{-2}, respectively, for 6 MV and corresponding values of $(0.9701\pm0.4\times10^{-3})$, $(0.48\times10^{-3}\pm0.1\times10^{-4})$ cm^{-1}, and $(0.67\times10^{-5}\pm0.4\times10^{-6})$ cm^{-2}, respectively, for 15 MV. The change in monitor backscatter factor from 5-cm square collimator setting to 40-cm square collimator setting was 2% for 6 MV and 3% for 15 MV.

C. Parametrization with the equivalent square at flattening filter

In Fig. 4, measured S_h are plotted against the side of the equivalent square of the luminous region. The maximum deviation was 0.9% for both 6 and 15 MV. The down stream shift t_e of the effective source in Eq. (7) was determined to be 0.9 cm for 6 MV and 0.4 cm for 15 MV.

D. Parametrization with the integral of the radial distribution

The piecewise linear scattered radiation radial distribution at the level of the flattening filter for both 6 and 15 MV are shown in Fig. 5. In Fig. 6, the measured relative fluence factors are compared with that from the integral of the radial

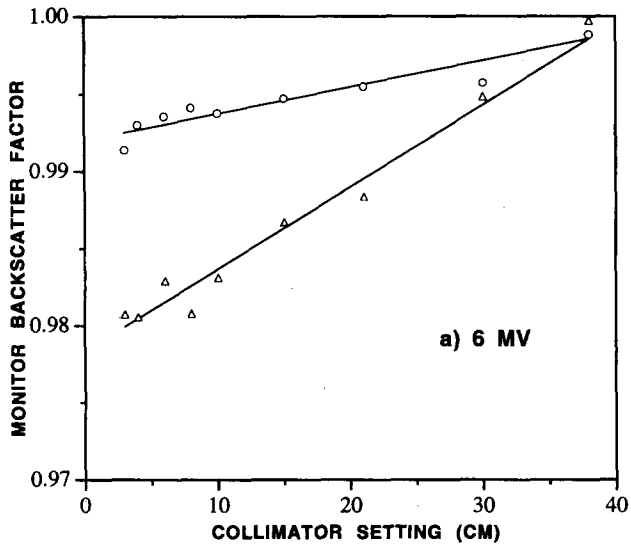

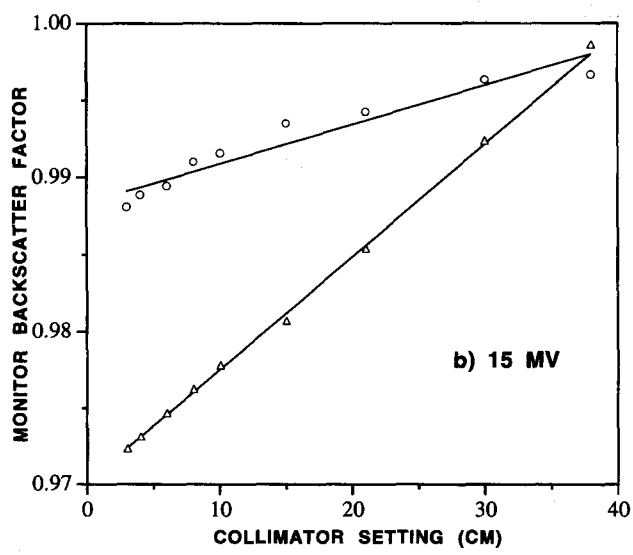

FIG. 3. Monitor backscatter factor for different upper jaw settings (triangles) and different lower jaw settings (circles). When a set of jaws was varied, the other set was kept at 38 cm. The solid lines are least squares fittings of a bilinear equation to the data as described in the text.

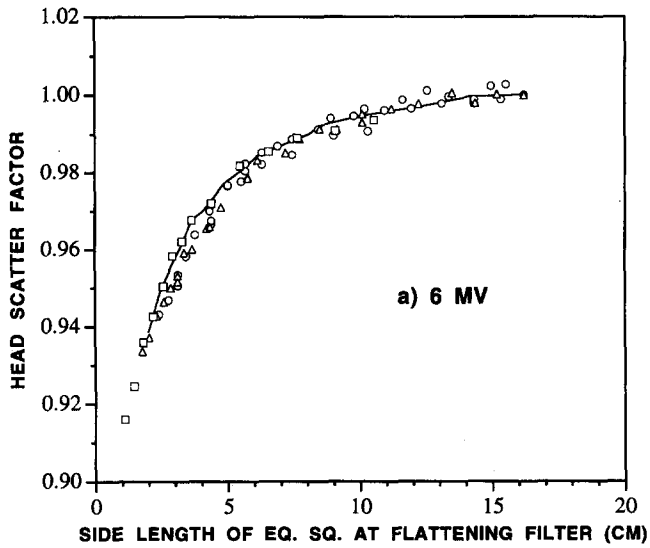

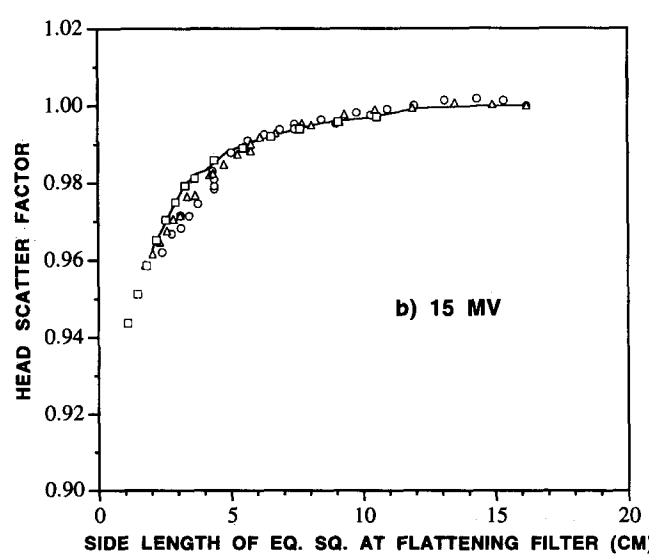

FIG. 4. Head scatter factor S_h for the data set shown in Fig. 2. The abscissa is the side length of the equivalent square of the luminous region. Symbols have the same interpretation as that of Fig. 2.

distribution using Eq. (8). At 100 cm, the maximum deviation was 0.4% for 6 MV and 0.3% for 15 MV. The maximum deviations were 0.5% and 0.9% for 6 and 15 MV, respectively, at 160 cm. Notice that the maximum deviation occurred at extended distance for the smallest field size such that the method was performing extrapolation of the radial distribution to smaller radii in the integration instead of interpolation from the measurements at 100 cm *SPD*. For the subset of data using interpolation, i.e., the subset of data such that the luminous regions were larger than that of the smallest field size at 100 cm, the maximum deviation was less than 0.5% for both 6 and 15 MV.

IV. DISCUSSION

We have parametrized three different methods with the same dataset of square fields and we have compared results of parametrization to measurements of various field configurations at different distances. For the two methods based on equivalent squares, their accuracy for square fields depends only on the interpolation method or curve fitting method employed. For the method based on the estimation of radial distribution of scattered radiation, the solution from singular value decomposition deviated less than 0.1% from the spline fitting to the square field data at 100-cm *SPD*. Thus, it is also limited only by the curve fitting method used.

For other field configurations, the traditional method of parametrizing S_c as a function of equivalent square at isocenter showed systematic deviation of the data from the parametrized S_c (Fig. 2). The deviation is partly due to backscatter into the monitor chamber. The changes in monitor backscatter factor (S_b) from 5-cm square collimator setting

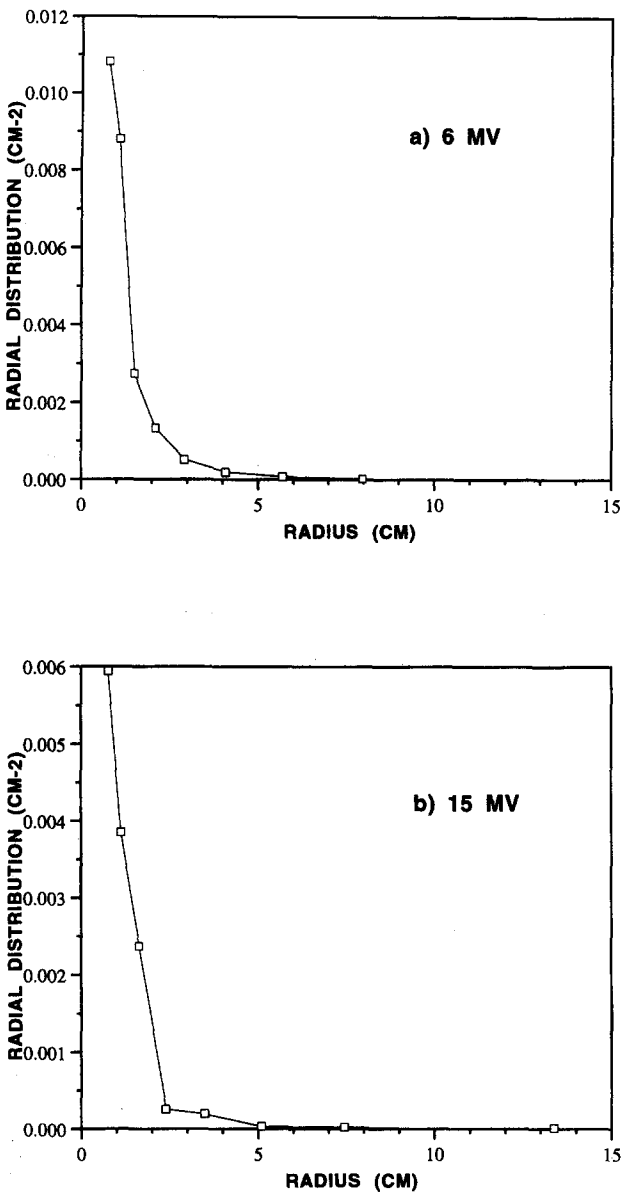

FIG. 5. Radial distribution of scattered radiation for 6 and 15 MV at the level of the flattening filter computed from square field measurements at isocenter.

to 40-cm square collimator setting (2% for 6 MV and 3% for 15 MV) are consistent with the results of Duzenli *et al.*[21] (2.5% for 6 MV and 4% for 18 MV of a Clinac 2100 C equipped with a Kapton monitor chamber). By comparing the percentage change in the data of rectangular fields from the smallest to the largest field sizes in Figs. 2 and 3, it can be seen that about 1/4 of the change is due to S_b for 6 MV. For 15 MV, about 1/2 of the change is due to S_b.

Both the equivalent square at flattening filter method and the radial distribution of scattered radiation method predicted the collimator scatter factor accurately. The former method has the advantage that it is simpler computationally than the latter method and hand calculation is feasible if tables of the data are available. It can be seen by comparing Figs. 4 and 6 that the latter method is slightly more accurate. However, as reported in Sec. III, the method based on radial distribution did not perform as well when extrapolation to small radii was necessary. Measurements at extended distance need to be included in the determination of the radial distribution if accuracy of small field size at extended distance is required.

The radial distributions estimated in this study depend on the first derivative of the measured S_c for square fields. So, it is expected to be more sensitive to variation of the data. We have found that the magnitude and shape of the radial distribution changes significantly for different splines fitted to the same data while the root-mean-square deviations between the fitted splines and the data are within experimental error. Further study is required to improve the precision of the determination of the radial distribution. The radial distribution determined in this study is qualitatively in agreement with that determined by Jaffray *et al.*[17]

Sharpe *et al.*[18] estimated collimator scatter factors of square and rectangular fields for 6 MV at 100 cm successfully from measured radial distributions. The radial distribution at the target was measured with a scanning slit, and radial distribution at the flattening filter was measured with special circular collimators. We have developed a method so that conventional square field measurements can be used to estimate the radial distribution. We have found that correction for backscatter into the monitor chamber improves the consistency between computed S_c and measured data. Also, we have extended their comparison to datasets at extended distance by showing that deviation from inverse-square-law of a point source at the target can be accurately predicted from separate inverse-square-law correction of the two sources in the model. Effective source distance measurement is not necessary.

The equivalent square at the flattening filter method performed well with rectangular visible regions at the level of the flattening filter, i.e., rectangular luminous regions. Further study needs to be done on the accuracy of the method for irregular luminous regions. However, most of the clinical situations will have rectangular regions for the following geometrical reason. If the adjustable collimators and a field-shaping block define the same field size at the isocenter, the physical opening of the collimators will be smaller than the physical opening of the field-shaping block because the collimators are closer to the target. Moreover, the visible region at the flattening filter defined by the collimators will be smaller than that defined by the field-shaping blocks, even if they have the same physical openings, because the collimators are closer to the flattening filter. Therefore, the luminous region will be rectangular, as defined by the adjustable collimators, unless the field size of the field-shaping blocks is much smaller than that of the adjustable collimators. For example, for a calculation point at the isocenter on a Varian Clinac with independent upper and lower jaws and a target to shadow tray distance of 65.4 cm, the field size at isocenter defined by the field-shaping block needs to be less than 0.28 times the upper jaw setting or 0.43 times the lower jaw setting to affect the luminous region. For linear accelerators

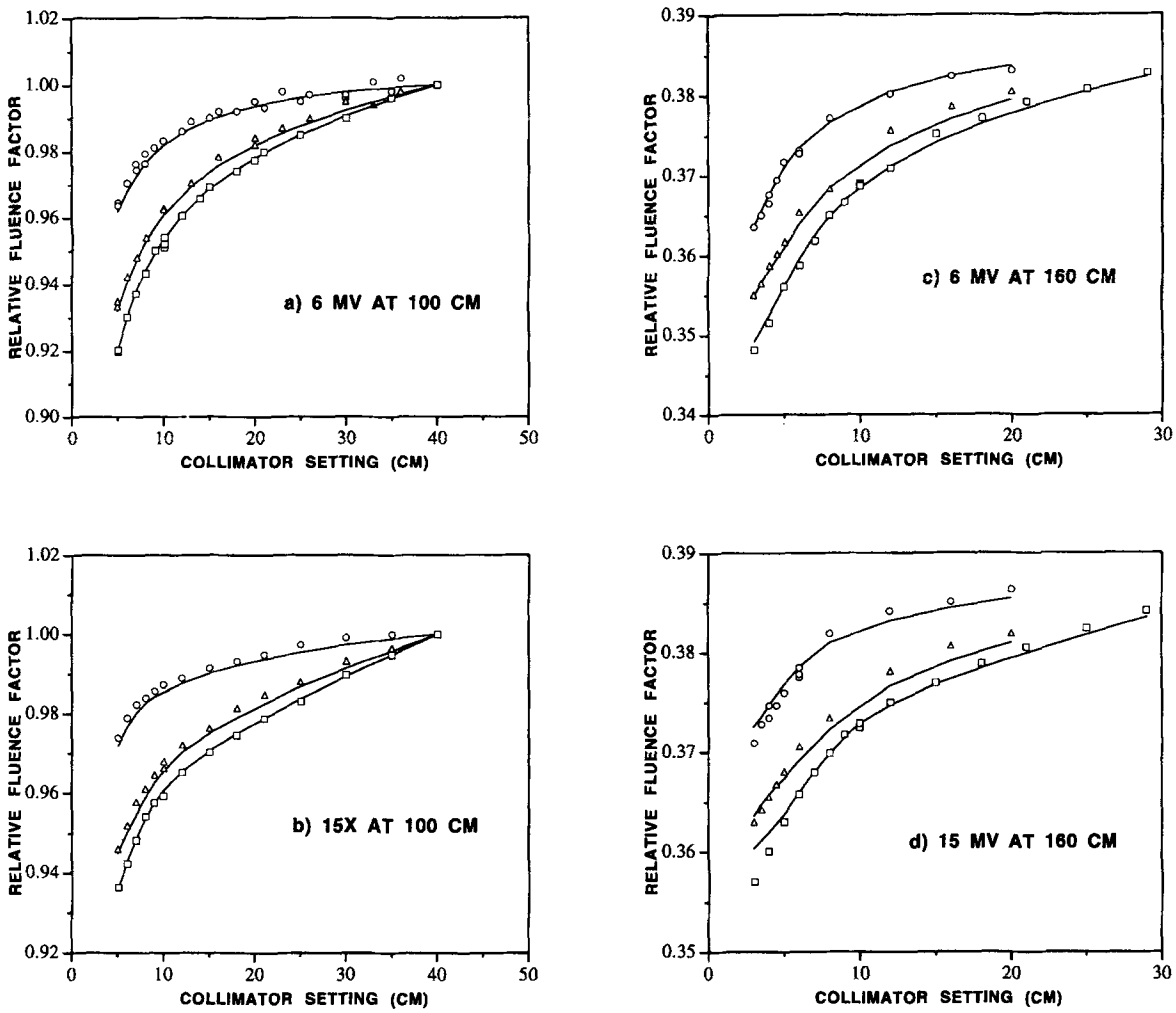

FIG. 6. Comparison of measured relative fluence factor (*RFF*) and computed *RFF*. Squares are measured *RFF*s of square fields, triangles are measured *RFF*s of rectangular fields of different upper jaw settings, and circles are measured *RFF*s of rectangular fields of different lower jaw settings. For rectangular field sizes, one set of jaws was varied while the other set was kept at 40 cm. Solid lines are computed *RFF*.

with the multileaf collimator next to the flattening filter, further measurements are needed to confirm the applicability of the equivalent square at the flattening filter method.

V. CONCLUSIONS

We have developed a method based on equivalent square at the flattening filter and a method based on a piecewise linear approximation of the radial distribution of scattered radiation at the level of the flattening filter to model the head scatter factor. The method employing radial distribution is slightly more accurate for rectangular fields. Both methods require measurements with square field sizes only. The method based on equivalent square at the flattening filter is especially attractive clinically due to its simplicity in computation.

ACKNOWLEDGMENTS

We would like to thank Steven Hardybala for machining the solid water mini-phantom. We are grateful to the referees for helpful suggestions. This work was supported in part by NIH Grant No. P01-CA59827.

APPENDIX A: MONITOR BACKSCATTER FACTOR

As suggested by Ahnesjo *et al.*[15] we have assumed that the amount of backscatter from a back surface of a collimator jaw is proportional to the irradiated surface area.

Thus,

$$I_m = I_f + a_1(L - r_y) + a_2 r_y (L - r_x), \tag{A1}$$

where I_m is the charge detected by the monitor chamber per unit electron charge landing on the target, L is the maximum collimator setting, a_1 and a_2 are constants, and I_f is the

monitor chamber current that is unrelated to backscatter. The electron charge landing on the target per monitor unit is

$$\frac{Q_{mu}}{I_m}=\frac{Q_{mu}}{I_0+b_1r_y+b_2r_xr_y}, \tag{A2}$$

where Q_{mu} is the charge collected by the monitor chamber per monitor unit; I_0, b_1, and b_2 are constants obtained from simplification of Eq. (A1). Since the percentage change in Q_{mu}/I_m when r_x and r_y changes from 0 to 40 cm is usually small, i.e., $\delta(r_x,r_y)\equiv b_1r_y+b_2r_xr_y$ is small compared to I_0, we may use a first-order approximation for Q_{mu}/I_m:

$$\begin{aligned}\frac{Q_{mu}}{I_m}&=\frac{Q_{mu}}{I_0+\delta(r_x,r_y)}\\&\cong\frac{Q_{mu}}{I_0}-\frac{Q_{mu}}{I_0}\frac{\delta(r_x,r_y)}{I_0}\\&=\frac{Q_{mu}}{I_0}-\frac{Q_{mu}}{I_0}\frac{b_1}{I_0}r_y-\frac{Q_{mu}}{I_0}\frac{b_2}{I_0}r_xr_y.\end{aligned} \tag{A3}$$

Here S_b is proportional to Q_{mu}/I_m if we assume that photon energy fluence is proportional to electron charge landing on the target. Then S_b can be written to first-order approximation as

$$S_b=c_0+c_1r_y+c_2r_xr_y. \tag{A4}$$

Actually, the expression above is more general and does not depend on the assumption that backscatter is proportional to the area. Let

$$S_b=f(r_x,r_y), \tag{A5}$$

where f is an analytic function of r_x and r_y. We may expand f by Taylor expansion:

$$\begin{aligned}S_b=f(0,0)&+\frac{\partial f}{\partial r_x}r_x+\frac{\partial f}{\partial r_y}r_y+\frac{1}{2}\frac{\partial^2 f}{\partial r_x^2}r_x^2+\frac{\partial^2 f}{\partial r_x\partial r_y}r_xr_y\\&+\frac{1}{2}\frac{\partial^2 f}{\partial r_y^2}r_y^2+\cdots.\end{aligned} \tag{A6}$$

When the upper jaw is closed, i.e., $r_y=0$, S_b is independent of r_x because the backscatter from the lower jaws is blocked. Therefore, to first order of r_x and r_y,

$$S_b\cong f(0,0)+\frac{\partial f}{\partial r_y}r_y+\frac{\partial^2 f}{\partial r_x\partial r_y}r_xr_y, \tag{A7}$$

which is in the same form as Eq. (A4).

APPENDIX B: PHYSICAL INTERPRETATION OF λ_t AND $\lambda(R)$

From Eqs. (1) and (8), when $SPD=SPD_0$,

$$\lambda_t+\int_\sigma\int\lambda(R)dA=\frac{1}{S_b}\frac{Q_c(r_x,r_y,SPD_0)}{Q_c(r_0,r_0,SPD_0)}. \tag{B1}$$

For a given electron current landing on the target during beam on,

$$S_b=\tau(r_x,r_y)/\tau(r_0,r_0), \tag{B2}$$

where the τ's are beam on times for a given number of Moniter Units for the indicated field sizes. Therefore,

$$\lambda_t+\int_\sigma\int\lambda(R)dA=\frac{I_c(r_x,r_y,SPD_0)}{I_c(r_0,r_0,SPD_0)}. \tag{B3}$$

If we assume that the current collected by the chamber is proportional to the dose rate $\dot{D}$ at the measurement point inside the mini-phantom,

$$\begin{aligned}\lambda_t+\int_\sigma\int\lambda(R)dA&=\frac{\dot{D}_c(r_x,r_y,SPD_0)}{\dot{D}_c(r_0,r_0,SPD_0)}\\&\equiv\dot{D}_N(r_x,r_y,SPD_0)\end{aligned} \tag{B4}$$

for a given electron current landing on the target. Thus, $\lambda(R)$ is the contribution to the normalized dose rate $\dot{D}_N$ from an area dA at radius R on the flattening filter to the point at the isocenter inside the mini-phantom. Similarly, λ_t is the contribution to the normalized dose rate from the point source at the target to the point at isocenter inside the mini-phantom. Since the dose from the filter is due to scattered radiation, $\lambda(R)$ is effectively the "radiance" of scattered radiation source at the flattening filter as seen through the mini-phantom. Effectively λ_t is the "radiant intensity" of the point source at the target as seen through the mini-phantom. Here $\lambda(R)$ has the dimension of area^{-1} and λ_t is just a dimensionless number because of the normalization.

APPENDIX C: NUMERICAL SOLUTION OF THE INTEGRAL EQUATION FOR RELATIVE FLUENCE FACTOR

To obtain $\lambda(R)$ from the discrete-cubic-spline fitting $q(\sigma)$, we solved Eq. (9) numerically. Since we were solving $\lambda(R)$ from the spline fitting, we were not limited to measured q. From the spline fitting, we generated a new series of q_i corresponding to a series of σ_i, $i=1,\ldots,m$. The m fitted q's included the fitted q of field sizes used in the measurement and nine fitted q's of field sizes between each consecutive measured field size. Thus we increased m to about ten times the number used in the measurement. Besides interpolation with the spline, we extrapolated $q(\sigma)$ to a field size that was half of the smallest measured field size and extrapolated to a field size twice the largest measured field size with the spline. The second derivatives were zero at the free ends of the spline, fitting so that the extrapolations were simple linear extrapolations.

We then approximated $\lambda(R)$ by a piecewise linear function. That is, for a given sequence of radii in ascending order, $R_i,\ldots,R_j,\ldots,R_n$, $\lambda(R)$ is a linear function between R_j and R_{j+1}. For radii between R_0 and R_1, where $R_0=0$, $\lambda(R)$ was taken to be constant. Thus, the piecewise linear approximation of $\lambda(R)$ is completely specified by $\lambda(R_j)$, $j=1,\ldots,n$ for $R_0<R<R_n$. If we define $\lambda_0\equiv\lambda_t$ and $\lambda_j\equiv\lambda(R_j)$, $j=1,\ldots,n$, it is shown in Appendix D that q_i can be written as

$$q_i=\sum_{j=0}^{n} M_{ij}\lambda_j, \tag{C1}$$

where M_{ij} depends only on the known geometry and field configuration of the in-air measurement.

Here λ_j can be determined in terms of q_i by finding the inverse of M_{ij}. In this study, the inverse of M_{ij} was determined by singular value decomposition.[23] It has the advantage that the algorithm can handle an overdetermined system of linear equations.

In the determination of the radial distribution, a geometric sequence of radii was chosen. That is, R_{j+1}/R_j=constant. The number of radii, n, was chosen to be $\frac{1}{20}$ of m, the number of q_i, to force the system of equations to be overdetermined.

APPENDIX D: REDUCTION OF THE INTEGRAL EQUATION TO A SYSTEM OF LINEAR EQUATIONS

An algebraic expression for the piecewise linear function $\lambda(R)$ is

$$\lambda(R)=\begin{cases}\lambda(R_1) & \text{for } R_0<R<R_1,\\ \lambda(R_{j-1})\left(\dfrac{R_j-R}{R_j-R_{j-1}}\right)+\lambda(R_j)\left(\dfrac{R-R_{j-1}}{R_j-R_{j-1}}\right)\\ \qquad \text{for } R_{j-1}<R<R_j \quad \text{and} \quad 2<j<n.\end{cases} \tag{D1}$$

If we define functions f_j, $j=1,\ldots,n$ such that

$$f_1\equiv\begin{cases}1 & \text{for } R_0<R<R_1,\\ \dfrac{R_2-R}{R_2-R_1} & \text{for } R_1<R<R_2,\\ 0 & \text{elsewhere,}\end{cases}$$

$$f_j\equiv\begin{cases}\dfrac{R-R_{j-1}}{R_j-R_{j-1}} & \text{for } R_{j-1}<R<R_j,\\ \dfrac{R_{j+1}-R}{R_{j+1}-R_j} & \text{for } R_j<R<R_{j+1}, \quad \text{where } 2<j<n-1,\\ 0 & \text{elsewhere,}\end{cases}$$

$$f_n\equiv\begin{cases}\dfrac{R-R_{n-1}}{R_n-R_{n-1}} & \text{for } R_{n-1}<R<R_n,\\ 0 & \text{elsewhere,}\end{cases}$$

then

$$\lambda(R)=\sum_{j=1}^{n}\lambda(R_j)f_j(R). \tag{D2}$$

Substituting this into Eq. (9),

$$q_i=\left(\frac{SPD_0}{SPD_i}\right)^2\lambda_t+\sum_{j=1}^{n}\left[\left(\frac{SPD_0-t_f}{SPD_i-t_f}\right)^2\int\int_{\sigma_i} f_j(R)dA\right]\lambda(R_j). \tag{D3}$$

If we define

$$\lambda_0\equiv\lambda_t,$$

$$M_{i0}\equiv\left(\frac{SPD_0}{SPD_i}\right)^2,$$

and

$$\lambda_j\equiv\lambda(R_j),$$

$$M_{ij}\equiv\left(\frac{SPD_0-t_f}{SPD_i-t_f}\right)^2\int\int_{\sigma_i} f_j(R)dA \quad \text{for } j=1,2,\ldots,n,$$

then

$$q_i=\sum_{j=0}^{n} M_{ij}\lambda_j.$$

[1] J. G. Holt, J. S. Laughlin, and J. P. Moroney, "The extension of the concept of tissue–air–ratios (TAR) to high-energy x-ray beams," Radiology **96**, 437–446 (1970).

[2] F. M. Khan, W. Sewchand, J. Lee, and J. F. Williamson, "Revision of tissue-maximum ratio and scatter-maximum ratio concepts for cobalt-60 and higher energy x-ray beams," Med. Phys. **7**, 230–237 (1980).

[3] J. J. M. van Gasteren, S. Heukelom, H. J. van Kleffens, R. van der Laarse, J. L. M. Venselaar, and C. F. Westermann, "The determination of phantom and collimator scatter components of the output of megavoltage photon beams: measurement of the collimator scatter part with a beam-coaxial narrow cylindrical phantom," Radiother. Oncol. **20**, 250–257 (1991).

[4] M. Tatcher and B. Bjarngard, "Head-scatter factors and effective x-ray source positions in a 25-MV linear accelerator," Med. Phys. **19**, 685–686 (1992).

[5] R. F. Moyer, "Systematic patient-dose errors for 4- and 10-MeV microwave linear accelerators associated with rectangular collimator settings," Radiology **129**, 803–806 (1978).

[6] M. S. Patterson and P. C. Shragge, "Characteristics of an 18-MV photon beam from a Therac 20 medical linear accelerator," Med. Phys. **8**, 312–318 (1981).

[7] K. R. Kase and G. K. Svensson, "Head scatter data for several linear accelerators (4–18 MV)," Med. Phys. **13**, 530–532 (1986).

[8] P. D. Higgins, W. H. Sohn, C. H. Sibata, and W. A. McCarthy, "Scatter factor corrections for elongated fields," Med. Phys. **16**, 800–802 (1989).

[9] W. Szymczyk, A. Goraczko, and J. Lesiak, "Prediction of Saturne II+ 10 MV and 23 MV photon beam output factors," Int. J. Radiat. Oncol. Biol. Phys. **21**, 789–793 (1991).

[10] M. Tatcher and B. E. Bjarngard, "Head-scatter factors in rectangular photon fields," Med. Phys. **20**, 205–206 (1993).

[11] R. Mohan, C. Chui, and L. Lidofsky, "Energy and angular distribution of photons from medical linear accelerators," Med. Phys. **12**, 592–597 (1985).

[12] P-H. Huang, J. Chu, and B. E. Bjarngard, "The effect of collimator backscatter radiation on photon output of linear accelerators," Med. Phys. **14**, 268–269 (1987).

[13] G. Luxton and M. A. Astrahan, "Output factor constituents of a high-energy photon beam," Med. Phys. **15**, 88–91 (1988).

[14] E. L. Chaney and T. J. Cullip, "A Monte Carlo study of accelerator head scatter," Med. Phys. **21**, 1383–1390 (1994).

[15] A. Ahnesjo, T. Knoos, and A. Montelius, "Application of the convolution method for calculation of output factors for therapy photon beams," Med. Phys. **19**, 295–301 (1992).

[16] P. B. Dunscombe and J. M. Nieminen, "On the field-size dependence of relative output from a linear accelerator," Med. Phys. **19**, 1441–1444 (1992).

[17] D. A. Jaffray, J. J. Battista, A. Fenster, and P. Munro, "X-ray sources of medical linear accelerators: Focal and extra-focal radiation," Med. Phys. **20**, 1417–1427 (1993).

[18] M. B. Sharpe, D. A. Jaffray, P. Munro, and J. J. Battista, "Photon dose calculations that include the focal and extra-focal radiation emitted by a linear accelerator," *Proceedings of the XIth International Conference on the Use of Computers in Radiation Therapy* (North Western Medical Physics Department, Christie Hospital NHS Trust, Manchester, M20 9BX, UK, 1994).

[19]A. Ahnesjo, "Analytic modelling of photon scatter from flattening filter in photon therapy beams," Med. Phys. **21**, 1227–1235 (1994).

[20]H. Kubo, "Telescopic measurements of backscattered radiation from secondary collimator jaws to a beam monitor chamber using a pair of slits," Med. Phys. **16**, 295–298 (1989).

[21]C. Duzenli, B. McClean, and C. Field, "Backscatter into the beam monitor chamber: Implications for dosimetry of asymmetric collimators," Med. Phys. **20**, 363–367 (1993).

[22]A. L. McKenzie and P. H. Stevens, "How is photon head scatter in a linear accelerator related to the concept of a virtual source?," Phys. Med. Biol. **38**, 1173–1180 (1993).

[23]W. H. Press, B. P. Flannery, S. A. Teukolosky, and W. T. Vetterling, *Numerical Recipes* (Cambridge University Press, New York, 1986).